13 Fundamentals of Chargers

Fariborz Musavi

CONTENTS

13.1 INTRODUCTION

As the demand for energy drastically increased in the twentieth century, fossil fuels became the main source of energy due to convenience and cost. Over the years, however, the price of oil and problems caused by pollution have increased considerably, putting pressure on governments and industries to invest on other solutions to replace fossil fuels. Consequently, interest in other means of transportation, such as plug-in hybrid electric vehicles (PHEVs) and electric vehicles (EVs), has increased again.

EV technology has existed since the early 1900s. However, the high cost and low energy density of available energy storage systems, primarily batteries, along with the very low cost of oil, had limited the interest in EV and PHEV. Recent innovations in lithium-ion batteries, higher price of gas, and air pollution associated with fossil fuels have significantly impacted the alternative transportation industry.

As a result, PHEVs and EVs are an emerging trend in automotive circles, and consumer's interest is growing rapidly. With the development of PHEVs and EVs, battery chargers for automotive applications are also becoming an essential part of transportation electrification. In addition, the improvement of overall charger efficiency and cost are critical for the emergence and acceptance of these vehicular technologies; as the charger efficiency increases, the charge time and utility cost decreases.

In this chapter, several conventional PHEV charger front-end AC–DC converter topologies and isolated DC–DC topologies are reviewed. Considerations to improve the efficiency and performance, which is critical to minimize the charger size, charging time, and the amount and cost of electricity drawn from the utility, are discussed. A detailed practical example along with an analytical model for these topologies is developed, along with various questions and homework assignments at the end of the chapter.

13.2 CHARGER CLASSIFICATION AND STANDARDS

A PHEV is a hybrid vehicle with a storage system that can be recharged by connecting a plug to an external electric power source through an AC or DC charging system. The AC charging system is commonly an on-board charger mounted inside the vehicle and is connected to the grid. The DC charging system is commonly an off-board charger mounted at fixed locations, supplying required regulated DC power directly to the batteries inside the vehicle.

13.2.1 AC Charging Systems

The charging AC outlet inevitably needs an on-board AC–DC charger with a power factor correction (PFC). Table 13.1 illustrates charge method electrical ratings according to SAE EV AC charging power levels.

These chargers are classified by the level of power they can provide to the battery pack [1]:

- Level 1: Common household circuit, rated up to 120 V AC and up to 16 A. These chargers use the standard three-prong household connection, and they are usually considered portable equipment.
- Level 2: Permanently wired electric vehicle supply equipment (EVSE) used especially for electric vehicle charging; rated up to 240 V AC, up to 60 A, and up to 14.4 kW.

TABLE 13.1
Charge Method Electrical Ratings—SAE EV AC Charging Power Levels

Charge Method	Nominal Supply Voltage	Maximum Current	Branch Circuit Breaker Rating	Output Power Level
AC level 1	120 V AC, 1-phase	12 A	15 A	1080 W
	120 V AC, 1-phase	16 A	20 A	1440 W
AC level 2	208–240 V AC, 1-phase	16 A	20 A	3300 W
	208–240 V AC, 1-phase	32 A	40 A	6600 W
	208–240 V AC, 1-phase	≤80 A	Per NEC 635	≤14.4 kW

- Level 3: Permanently wired EVSE used especially for electric vehicle charging; rated greater than 14.4 kW. Fast chargers are rated as level 3, but not all level 3 chargers are fast chargers. This designation depends on the size of the battery pack to be charged and how much time is required to charge the battery pack. A charger can be considered a fast charger if it can charge an average electric vehicle battery pack in 30 min or less.

In summary

- AC chargers are commonly on-board the vehicle
  - AC is supplied to the vehicle
  - Charger supplies DC to the battery
  - Must be automotive-grade components
- Considerations for reliability, thermal cycling, vibration, lifetime/warranty, and so on
- High cost to produce and low profit margins for suppliers
- AC levels 1 and 2 are the dominant technologies in production today

13.2.2 DC Charging Systems

The DC charging systems are mounted at fixed locations, like the garage or dedicated charging stations. Built with dedicated wiring, these chargers can handle much more power and can charge the batteries more quickly. However, as the output of these chargers is DC, each battery system requires the output to be changed for that car. Modern charging stations have a system for identifying the voltage of the battery pack and adjusting accordingly. Table 13.2 illustrates charge method electrical ratings according to SAE EV DC charging power levels.

These chargers are classified by the level of power they can provide to the battery pack [1]:

- Level 1: Permanently wired EVSE includes the charger; rated 200–450 V DC, up to 80 A, and up to 36kW

TABLE 13.2
Charge Method Electrical Ratings—SAE EV DC Charging Power Levels

Charge Method	Supplied DC Voltage Range	Maximum Current	Power Level
DC level 1	200–450 V DC	≤80 A DC	≤36 kW
DC level 2	200–450 V DC	≤200 A DC	≤90 kW
DC level 3	200–600 V DC	≤400 A DC	≤240 kW

- Level 2: Permanently wired EVSE includes the charger; rated 200–450 V DC, up to 200 A, and up to 90 kW
- Level 3: Permanently wired EVSE includes the charger; rated 200–600 V DC, up to 400 A, and up to 240 kW

In summary

- DC chargers are off-board (not in the vehicle)
  - AC supplied to a charging box
  - Charger supplies DC to the vehicle
- Consumer-grade components
  - Considerations for reliability, thermal cycling, vibration, and so on not as demanding
  - Lower cost to produce and potentially increased profit margins
- DC level 3 Tesla superchargers limited availability
- EVSE includes an off-board charger

13.3 CHARGER REQUIREMENTS

Several considerations and regulatory standards must be met. The charger must comply with the following standards for safety:

- UL 2202: EV Charging System Equipment
- IEC 60950: Safety of Information Technology Equipment
- IEC 61851-21: Electric Vehicle Conductive Charging System—Part 21: Electric Vehicle Requirements for Conductive Connection to an AC–DC Supply
- IEC 61000: Electromagnetic compatibility (EMC)
- ECE R100: Protection against Electric Shock
- ISO 6469-3: Electric Road Vehicles—Safety Specifications—Part 3: Protection of Persons against Electric Hazards
- ISO 26262: Road Vehicles—Functional Safety
- SAE J2929: Electric and Hybrid Vehicle Propulsion Battery System Safety Standard
- FCC Part 15 Class B: The Federal Code of Regulation (CFR) FCC Part 15 for EMC Emission Measurement Services for Information Technology Equipment

In addition, it may be affected by high temperatures, vibration, dust, and other parameters, which comprise the operating environment. Therefore, the charger must meet the following operating environment:

- Engine compartment capable
- IP6K9K, IP6K7 protection class
- −40°C to 105°C ambient air temperature
- −40°C to 70°C liquid coolant temperature

The input and output requirements for a level 2, 3.3 kW charger are also given below.
Input:

- Input voltage range: 85–265 VAC
- Input frequency range: 45–70 Hz
- Input current: 16 ARMS max
- Power factor: ≥0.98

Output:

- Output voltage range: 170–440 V DC
- Output power: 3.3 kW max
- Output current: 12 A DC max
- High efficiency: >94%

13.4 TOPOLOGY SELECTION FOR LEVEL 1 AND 2 AC CHARGERS

The front-end AC–DC converter is a key component of the charger system. A variety of circuit topologies and control methods have been developed for the PFC application [2,3]. The single-phase active PFC techniques can be divided into two categories: the single-stage approach and the two-stage approach. The single-stage approach is suitable for low-power applications. In addition, owing to large low-frequency ripple in the output current, only lead acid batteries are chargeable. Furthermore, galvanic isolation is required in on-board battery chargers in order to meet the double fault protection for the safety of the users of PHEV. Therefore, the two-stage approach is the proper candidate for PHEV battery chargers, where the power rating is relatively high, and lithium-ion batteries are used as the main energy storage system. The front-end PFC section is then followed by a DC–DC section to complete the charger system.

Figure 13.1 illustrates a simplified block diagram of a universal input two-stage battery charger used for PHEVs and EVs.

The PFC stage rectifies the input AC voltage and transfers it into a regulated intermediate DC link bus. At the same time, PFC function is achieved. The following DC–DC stage then converts the DC bus voltage into a regulated output DC voltage for charging batteries, which is required to meet the regulation and transient requirements.

13.4.1 Front-End AC–DC Converter Topologies

As a key component of a charger system, the front-end AC–DC converter must achieve high efficiency and high power density. Additionally, to meet the efficiency and power factor requirements and regulatory standards for the AC supply mains, PFC is essential.

As the adoption rate of these vehicles increases, the stress on the utility grid is projected to increase significantly at times of peak demand. Therefore, efficient and high power factor charging is critical in order to minimize the utility load stress, and reduce the charging time. In addition, a high power factor is needed to limit the input current harmonics drawn by these chargers and to meet regulatory standards, such as IEC 1000-3-2 [4].

According to the requirements of input current harmonics and output voltage regulation, a front-end converter is normally implemented by a PFC stage. Conventionally, most of the power conversion equipment employs either a diode rectifier or a thyristor rectifier with a bulk capacitor to

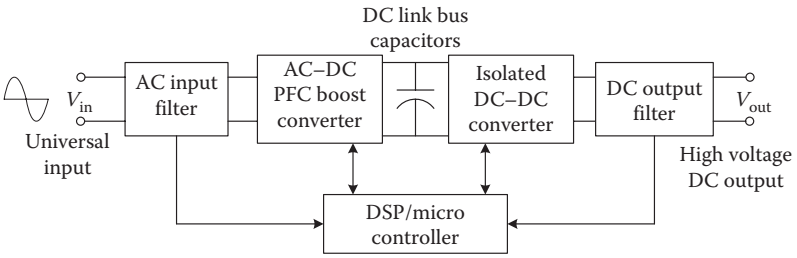

FIGURE 13.1 Simplified system block diagram of a universal on-board two-stage battery charger.

convert AC voltage to DC voltage before processing it. Such rectifiers produce input current with rich harmonic content, which pollute the power system and the utility lines. Power quality is becoming a major concern for many electrical users.

The simplest form of PFC is passive (passive PFC). A passive PFC uses a filter at the AC input to correct poor power factor. The passive PFC circuitry uses only passive components—an inductor and some capacitors. Although pleasantly simple and robust, a passive PFC rarely achieves low total harmonic distortion (THD). Furthermore, because the circuit operates at the low line power frequency of 50 or 60 Hz, the passive elements are normally bulky and heavy. Figure 13.2 shows input voltage and current for a passive PFC and the harmonic spectrum of input current.

The input power factor (PF) is defined as the ratio of the real power over apparent power as

$$\text{Power factor (PF)} = \frac{\text{Real power (W)}}{\text{Apparent power (VA)}} \tag{13.1}$$

Assuming an ideal sinusoidal input voltage source, the power factor can be expressed as the product of two factors, the distortion factor and the displacement factor, given as

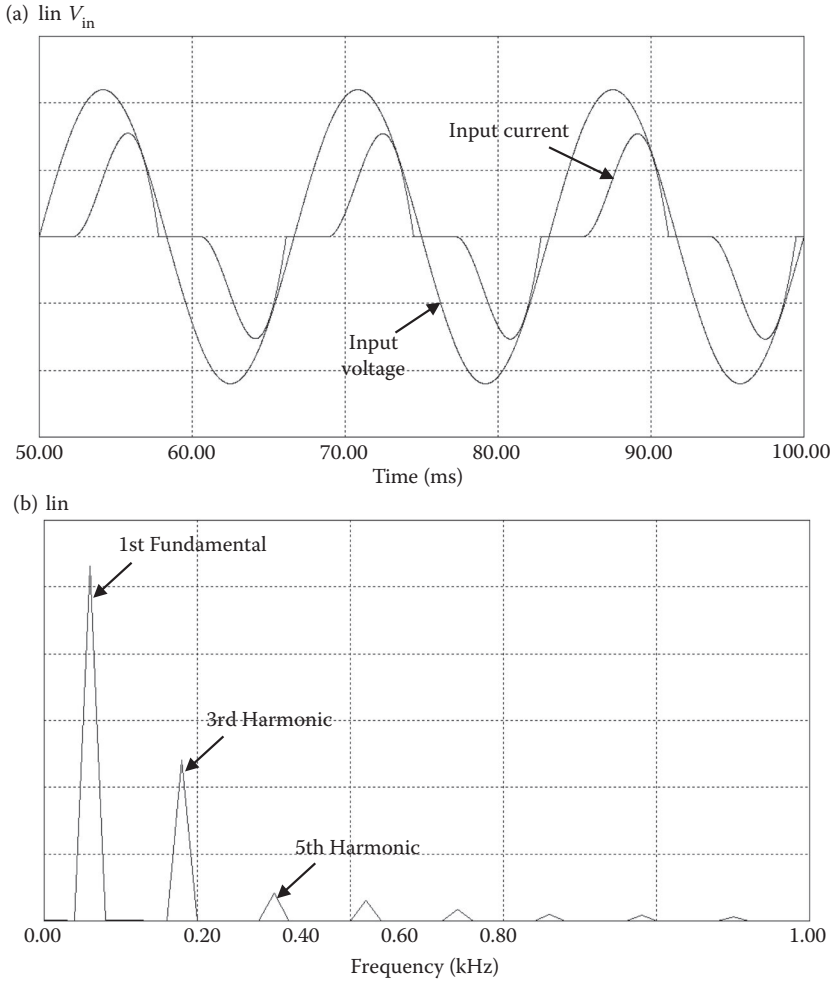

FIGURE 13.2 Passive power factor correction AC main voltage and current waveforms. (a) Input voltage and input current. (b) Harmonic spectrum of input current.

$$PF = K_d K_\theta \tag{13.2}$$

The distortion factor, K_d, is the ratio of the fundamental root mean square (RMS) current to the total RMS current.

a. Input voltage and input current
b. Harmonic spectrum of input current

The displacement factor, K_θ, is the cosine of the displacement angle between the fundamental input current and the input voltage fundamental RMS current.

$$K_d = \frac{I_{1\text{rms}}}{I_{\text{rms}}} \tag{13.3}$$

$$K_\theta = \cos \theta_1 \tag{13.4}$$

where $I_{1\text{rms}}$ is the fundamental component of the line current, I_{rms} is the total line current, and θ_1 is the phase shift of the current fundamental relative to the sinusoidal line voltage.

The distortion factor is close to unity, even for waveforms with noticeable distortion; therefore, it is not a very convenient measure of distortion for practical use. The distortion factor is uniquely related to another figure of merit: the THD.

$$\text{THD} = \sqrt{\frac{I_{\text{rms}}^2 - I_{1\text{rms}}^2}{I_{1\text{rms}}^2}} \tag{13.5}$$

$$K_d = \sqrt{\frac{1}{1 + \text{THD}^2}} \tag{13.6}$$

K_d is regulated by IEC 1000-3-2 for lower power levels and by IEEE Std 519-1992 [5] for higher power levels, where K_θ is regulated by utility companies.

Significant reduction of current harmonics in single-phase circuits can only be achieved by using rectifiers based on pulse width modulated (PWM) switching converters. These converters can be designed to emulate a resistive load and, therefore, produce very little distortion of the current. By using PWM or other modulation techniques, these converters draw a nearly sinusoidal current from the AC line in phase with the line voltage. As a result, the rectifier operates with very low current harmonic distortion and very high, practically unity power factor. This technique is commonly known as PFC. As a result of this research, the existing PFC technology based on the boost converter topology with average-current-mode control was significantly improved. The proposed improvements allowed an extended range of operating conditions and additional functionality. The following section illustrates several common PFC topologies suitable for PHEV charger applications.

13.4.1.1 Conventional Boost PFC Converter

The conventional boost topology is the most popular topology for PFC applications. It uses a dedicated diode bridge to rectify the AC input voltage to DC, which is then followed by the boost section, as shown in Figure 13.3.

In this topology, the output capacitor ripple current is very high and is the difference between diode current and the DC output current. Furthermore, as the power level increases, the diode bridge losses significantly degrade the efficiency, so dealing with the heat dissipation in a limited area

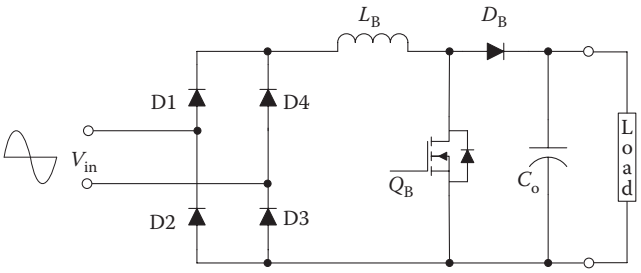

FIGURE 13.3 Conventional PFC boost converter.

becomes problematic. The inductor volume also becomes a problematic design issue at high power. Another challenge is the power rating limitation for current sense resistors at high power.

13.4.1.2 Interleaved Boost PFC Converter

The interleaved boost converter, illustrated in Figure 13.4, consists of two boost converters in parallel operating at 180° out of phase [6–8].

The input current is the sum of the two input inductor currents. Because the inductors' ripple currents are out of phase, they tend to cancel each other and reduce the input ripple current caused by the boost switching action. The interleaved boost converter has the advantage of paralleled semiconductors. Furthermore, by switching 180° out of phase, it doubles the effective switching frequency and introduces smaller input current ripple, so the input EMI filter is relatively small [9,10]. With ripple cancellation at the output, it also reduces stress on output capacitors.

13.4.1.3 Bridgeless Boost PFC Converter

The bridgeless boost topology, illustrated in Figure 13.5, is the second topology considered for this application. The gates of the powertrain switches are tied together, so the gating signals are identical, as is illustrated in Figure 13.6. It avoids the need for the rectifier input bridge, yet maintains

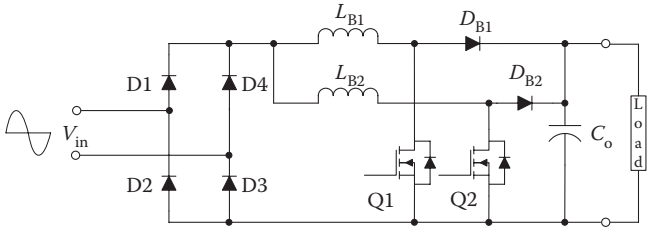

FIGURE 13.4 Interleaved PFC boost converter.

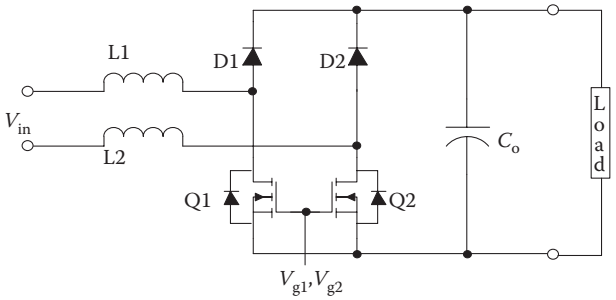

FIGURE 13.5 Bridgeless PFC boost topology.

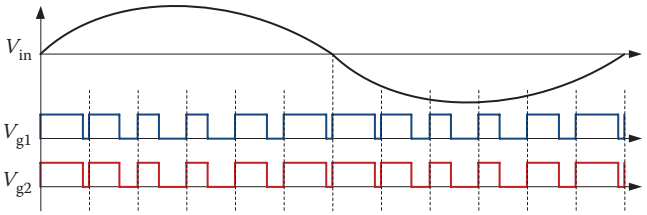

FIGURE 13.6 Gating scheme for the bridgeless PFC boost topology illustrating the identical gating signals for both MOSFETs.

the classic boost topology [11–14]. It is an attractive solution for applications >1 kW, where power density and efficiency are important. The bridgeless boost converter, also known as dual-boost PFC converter, solves the problem of heat management in the input rectifier diode bridge, but it introduces increased electromagnetic interference (EMI) [15–17]. This is because the amplitude of the noise source applied to the stray capacitor from high-voltage DC bus and power ground is a lot higher in bridgeless PFC; as a result, the common mode (CM) noise generated by bridgeless PFC is much higher than conventional boost PFC topology. Another disadvantage of this topology is the floating input line with respect to the PFC stage ground, which makes it impossible to sense the input voltage without a low-frequency transformer or an optical coupler.

13.4.1.4 Dual-Boost PFC Converter

The dual-boost converter, illustrated in Figure 13.7, is an alternative adaptation of the bridgeless boost topology [18]. In this topology, the MOSFET gates are decoupled, enabling one of the switches to remain on and operate as a synchronous MOSFET for half-line cycle. Figure 13.8 illustrates the gating scheme for a dual-boost PFC topology. The dual-boost topology reduces gate loss, and at light loads, conduction loss can be reduced until the voltage drop across the MOSFET channel $R_{DS(ON)}$ becomes equal to the voltage drop across the MOSFET body diode, at which point any additional current conducts through the body diode. The light load efficiency improvement comes at the expense of the cost of an additional driver and increased controller complexity.

13.4.1.5 Semi-Bridgeless Boost PFC Converter

The semi-bridgeless configuration, shown in Figure 13.9, includes the conventional bridgeless topology with two additional slow diodes, Da and Db, that connect the input to the PFC ground [19]. The slow diodes were added to address EMI-related issues [15,16]. The current does not always return through these diodes, so their associated conduction losses are low. This occurs since the inductors exhibit low impedance at the line frequency, so a large portion of the current flows through the MOSFET intrinsic body diodes. The semi-bridgeless configuration also resolves the floating input line problem with respect to the PFC stage ground. The topology change enables input voltage sensing using a string of simple voltage dividers.

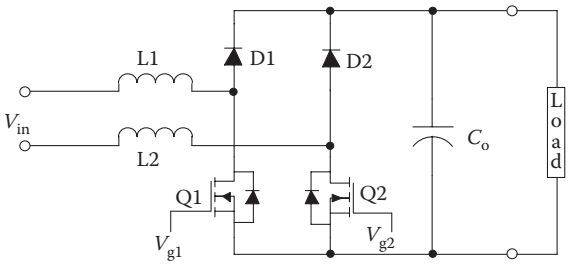

FIGURE 13.7 Dual-boost PFC topology.

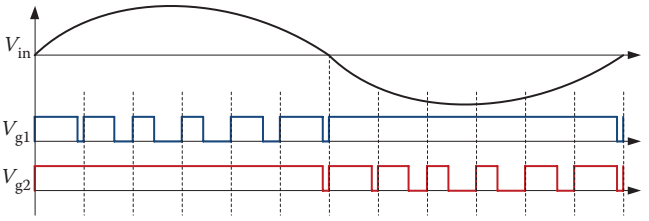

FIGURE 13.8 Gating scheme for the dual-boost PFC topology illustrating half-line cycle synchronous rectification.

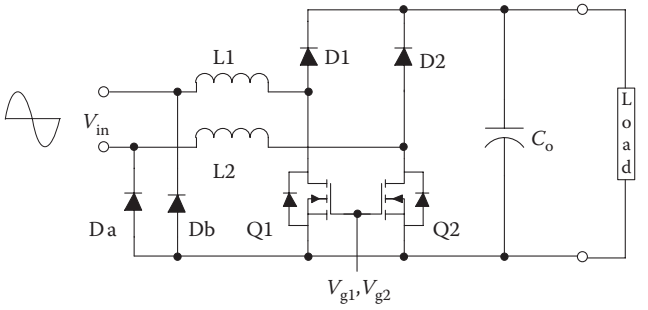

FIGURE 13.9 Semi-bridgeless PFC boost topology.

13.4.1.6 Bridgeless Interleaved Boost PFC Converter

The bridgeless interleaved topology, shown in Figure 13.10, was proposed as a solution to operate at power levels above 3.5 kW. In comparison to the interleaved boost PFC, it introduces two MOSFETs and also replaces four slow diodes with two fast diodes. The gating signals are 180° out of phase, similar to the interleaved boost. A detailed converter description and steady-state operation analysis are given in Reference 20. This converter topology shows a high input power factor, high efficiency over the entire load range, and low input current harmonics.

Since the proposed topology shows high input power factor, high efficiency over the entire load range, and low input current harmonics, it is a potential option for single-phase PFC in high-power level 2 battery charging applications.

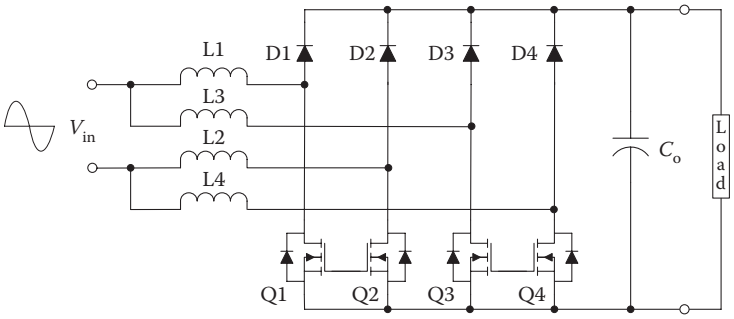

FIGURE 13.10 Bridgeless interleaved PFC boost converter. (From F. Musavi; W. Eberle; W.G. Dunford, *IEEE Transactions on Industry Applications*, 47, July/August 2011.)

13.4.2 Isolated DC–DC Converter Topologies

Many high-efficiency full-bridge DC–DC converter solutions have been proposed that are potential candidates for the isolated DC–DC converter in a PHEV charger. The DC–DC converter requirements for battery chargers are

- Galvanic isolation (regulatory requirement)
- Suitable for high power (>1 kW)
- High efficiency (>95%)
- Soft-switching (ZVS and zero current switching (ZCS)) (>100 kHz operation)
- Low EMI
- Low output voltage/current ripple (avoid battery heating)
- Small size
- Cost effective

13.4.2.1 Zero Voltage Switching Full-Bridge Phase-Shifted Converter

The phase-shifted zero voltage switching (ZVS) PWM DC-to-DC full-bridge converter, illustrated in Figure 13.11, was presented in References 21–23. ZVS for the switches is realized by using the leakage inductance of the transformer in addition to an external inductor and the output capacitance of the switch.

There are several issues with this topology. Although various improvements have been suggested for this converter, these solutions increase the component count and suffer from one or more disadvantages, including a limited ZVS range, high-voltage ringing on the secondary-side rectifier diodes, or duty cycle loss. The wide ZVS range of operation is discussed in References 24 and 25, and the high-voltage ringing on the secondary-side rectifier diodes is addressed in References 26–29. Duty cycle loss is reviewed in Reference 30. A new complementary gating scheme for the full-bridge DC-to-DC PWM converter is presented in Reference 31. This gating scheme requires an additional zero voltage transition (ZVT) circuit to achieve ZVS for all the switches for a wide variation in the load current. This topology is more suitable for low output voltage, high output current applications.

13.4.2.2 Zero Voltage Switching Full-Bridge Trailing-Edge PWM Converter

The full-bridge ZVS converter with trailing-edge PWM converter presented in Figure 13.12 behaves similar to a traditional hard-switched topology, but rather than simultaneously driving the diagonal bridge switches, the lower switches (Q3 and Q4) are driven at a fixed 50% duty cycle, and the upper switches (Q1 and Q2) are PWM on the trailing edge [32].

A clamp network consisting of D_C, R_C, and C_C is needed across the output rectifier to clamp the voltage ringing due to diode junction capacitance with the leakage inductance of the transformer. This DC–DC converter also suffers from duty cycle loss. Duty cycle loss occurs for converters

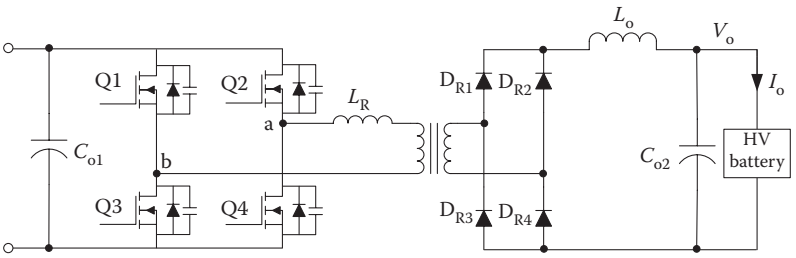

FIGURE 13.11 ZVS F.B. phase-shifted DC–DC converter topology.

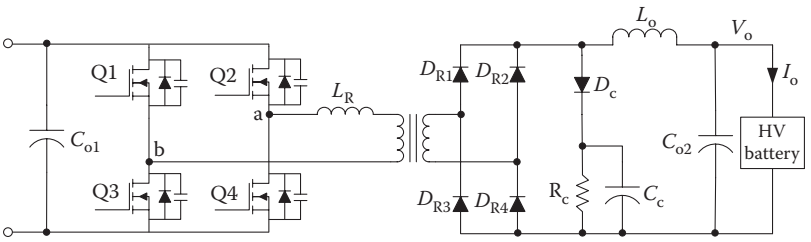

FIGURE 13.12 Improved ZVS F.B. trailing-edge DC–DC converter topology.

requiring inductive output filters when the output rectifiers commutate, enabling all of the diodes to conduct, which effectively shorts the secondary winding. This causes a decrease in the output voltage; thus, a higher transformer turn ratio is needed, which increases the primary peak current. This topology is also more suitable for low output voltage, high output current applications.

13.4.2.3 Zero Voltage Switching Full Bridge with Capacitive Output Filter Converter

The ZVS full-bridge converter topology with capacitive output filter is illustrated in Figure 13.13. Current-fed topologies with capacitive output filter inherently minimize diode rectifier ringing since the transformer leakage inductance is effectively placed in series with the supply-side inductor [33]. In addition, high efficiency can be achieved with ZVS; in particular, the trailing-edge PWM full-bridge gating scheme proposed in Reference 34 is an attractive solution to achieve ZVS.

The converter primary-side circuit consists of a traditional full-bridge inverter, but rather than driving the diagonal bridge switches simultaneously, the lower switches (Q3 and Q4) are driven at a fixed 50% duty cycle and the upper switches (Q1 and Q2) are pulse width modulated on the trailing edge. Although the proposed converter can operate in either discontinuous conduction mode (DCM), boundary conduction mode (BCM), or continuous conduction mode (CCM), only the DCM and BCM modes are desirable.

13.4.2.4 Interleaved Zero Voltage Switching Full Bridge with Capacitive Output Filter Converter, Operating in BCM

The current-fed topologies suffer from high ripple current stress at the output filter capacitors. The interleaved ZVS full bridge with capacitive output filter converter, illustrated in Figure 13.14, reduces the input and output filtering requirements and also reduces the reverse recovery losses in the secondary rectifier diodes.

An interleaved, multicell configuration that uses two cells (each rated at 1.65 kW) in parallel (at both input and output) with each cell being phase-shifted by 180° (=360°/2) is adopted for this high-power application [35]. Owing to interleaving, each cell shares equal power and the thermal losses are distributed uniformly among the cells and also the input/output ripple is four times the switching frequency.

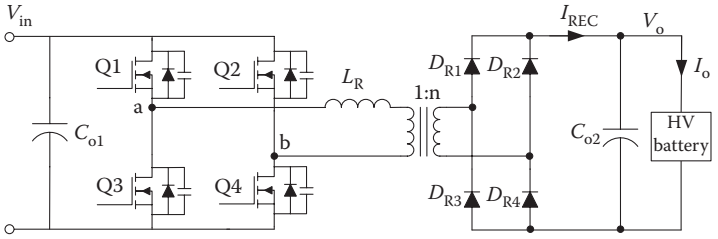

FIGURE 13.13 ZVS F.B. trailing-edge DC–DC converter topology with capacitive output filter.

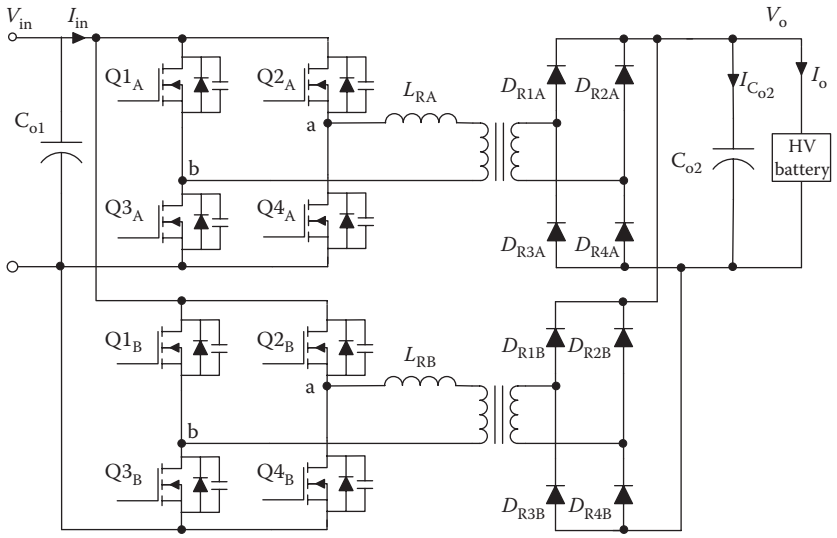

FIGURE 13.14 Interleaved ZVS F.B. trailing-edge DC–DC converter with capacitive output filter.

13.4.2.5 Interleaved Zero Voltage Switching Full Bridge with Voltage Doubler, Operating in BCM

An interleaved ZVS full bridge with voltage doubler, illustrated in Figure 13.15, is proposed to further reduce the ripple current and voltage stress on the output filter capacitors, as well as component cost reduction.

Owing to interleaving, each cell shares equal power and the thermal losses are distributed uniformly among the cells and also the input ripple is four times the switching frequency. Moreover, the output voltage doubler rectifier significantly reduces the number of secondary diodes and the voltage rating of the diodes is equal to the maximum output voltage [36].

Although the proposed converter can operate in either DCM, BCM, or CCM, only the DCM and BCM modes are desirable. Operation in CCM results in the lowest RMS currents and ZVS

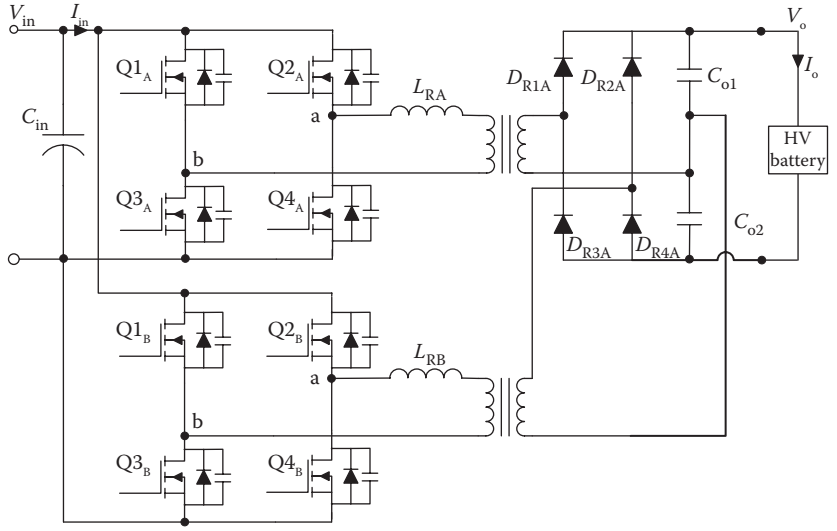

FIGURE 13.15 Interleaved ZVS F.B. trailing-edge DC–DC converter with voltage doubler.

can be achieved for all switches, but the high *di/dt* results in large reverse recovery losses in the secondary-side rectifier diodes and high-voltage ringing. Moreover, to operate this converter in CCM, it requires a larger resonant inductor, which also increases the transformer turns ratio and thus increases stress on the primary-side switches. Thus, this converter should be designed to operate in DCM, or BCM.

13.4.2.6 Full-Bridge LLC Resonant DC–DC Converter

Figure 13.16 illustrates a full-bridge LLC resonant converter. The LLC resonant converter is widely used in the telecom industry for its high efficiency at the resonant frequency and its ability to regulate the output voltage during the holdup time, where the output voltage is constant and the input voltage might drop significantly. However, the wide output voltage range requirements for a battery charger are drastically different and challenging compared to telecom applications, which operate in a narrow output voltage range.

Figure 13.17 illustrates a family of typical DC gain characteristics for an LLC converter as a function of normalized switching frequency for seven different load conditions varying from no-load to short circuit. Resonance occurs at unity gain, where the resonant capacitors and series resonant inductor are tuned.

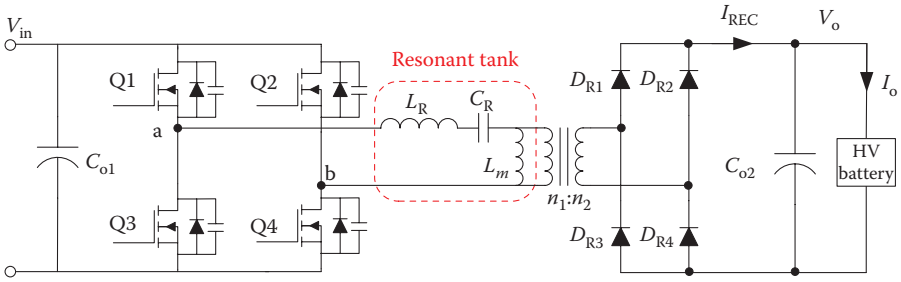

FIGURE 13.16 Full-bridge LLC resonant DC–DC converter topology.

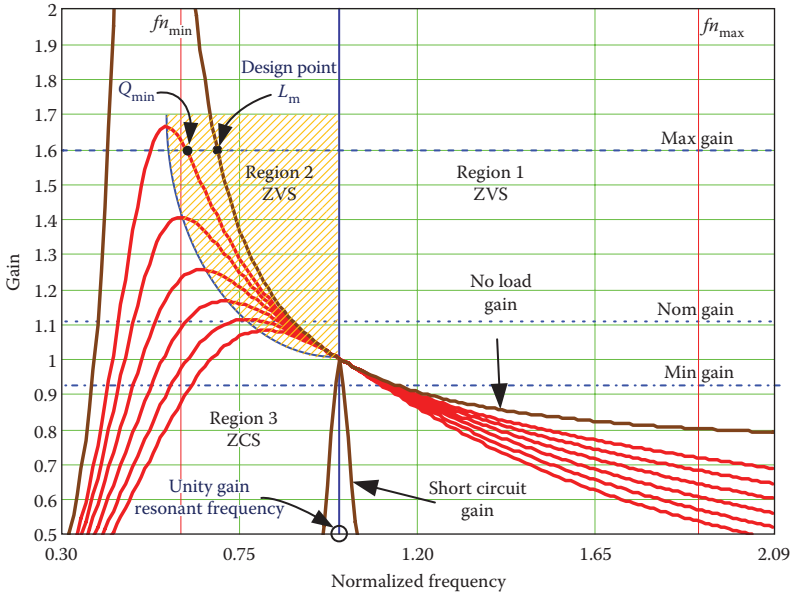

FIGURE 13.17 Typical DC gain characteristics of a LLC converter using FHA.

A detailed design procedure and resonant tank selection for LLC resonant converters in battery charging application is given in Reference 37.

13.5 TOPOLOGY SELECTION FOR LEVEL 3 CHARGERS

Level 3 chargers are mostly permanently wired EVSE used especially for electric vehicle charging and rated greater than 14.4 kW. These chargers are mainly off-board connected to a three-phase supply. Fast chargers are rated as level 3, but not all level 3 chargers are fast chargers. A charger can be considered a fast charger if it can charge an average electric vehicle battery pack in 30 min or less. This charger is also considered DC charger, since the interface between the charger and vehicle is through DC connector.

Figure 13.18 illustrates a typical block diagram for EV, PHEV charger level 3 using digital power controllers, communication devices, high-performance drivers, and interface devices [38].

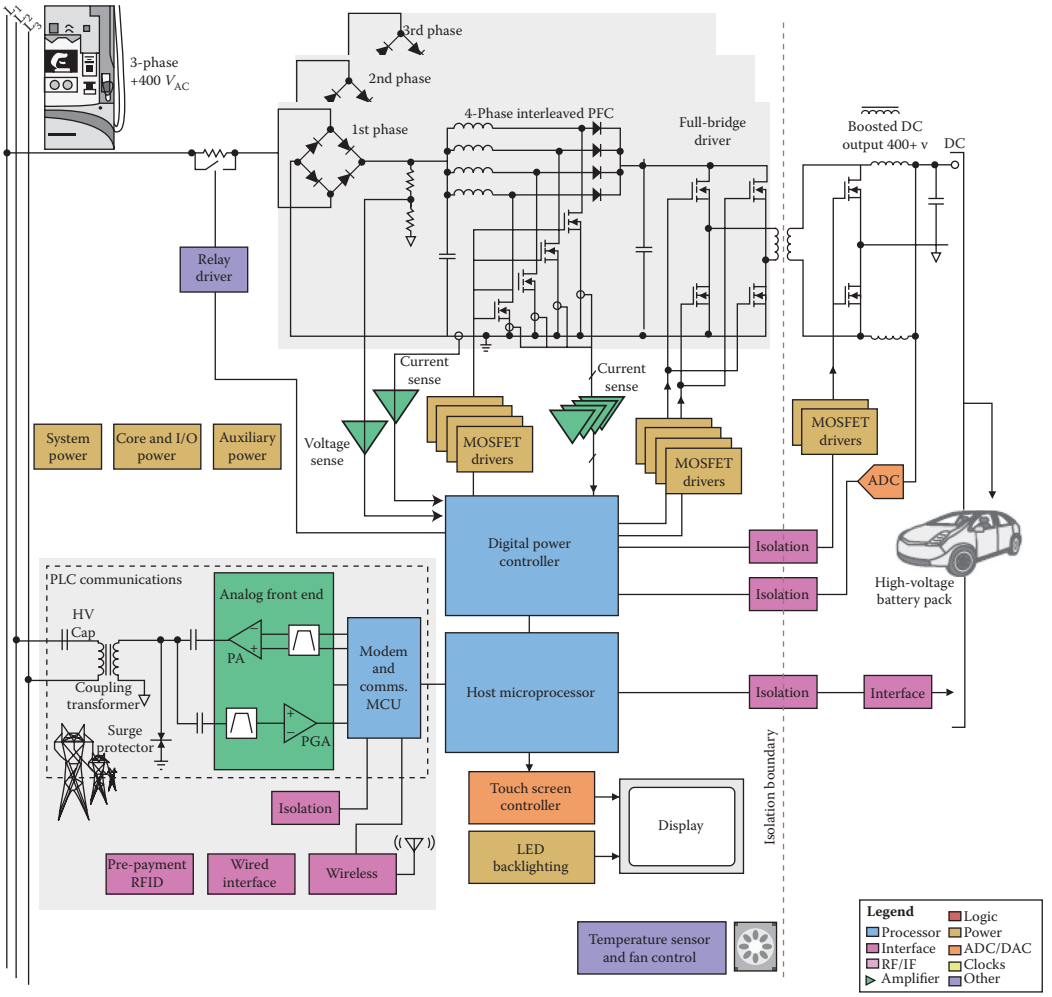

FIGURE 13.18 Typical block diagram for EV, PHEV charger level 3 using digital power controllers, communication devices, high-performance drivers, and interface devices. (From http://www.ti.com/solution/ev_hev_charger_level_3, Texas Instrument.)

As it can be noted, the supplied voltage to the charger is three-phase 400 V AC, so it requires a three-phase PFC converter for the mains interfaces, followed by a high-power high-voltage DC–DC converter(s).

13.5.1 Front-End AC–DC Converter Topologies

These EV chargers, supplied from three-phase AC lines, typically require a peak power ranging from 10 to 150 kW in order to inject direct current into the battery sets at variable voltage levels according to the vehicle (50–600 V).

The three-phase unity power factor converter options for the mains interface of high-power level 3 chargers are [39,40]:

a. Three single-phase PFC converters connected in Y or Δ configuration
b. Buck-type three-phase PFC rectifiers
c. Boost-type three-phase PFC rectifiers

A simple, reliable solution would be connecting three single-phase PFC boost converters in either Y or Δ configuration.

Buck-type three-phase PFC rectifiers, also known as current source rectifiers (CSRs), are appropriate for these high-power chargers as well, as a direct connection to the DC bus could be used.

Compared to the boost-type systems, buck-type topologies provide a wider output voltage control range, while maintaining PFC capability at the input and can potentially enable direct startup, while allowing for dynamic current limitation. In addition, three-phase boost-type rectifiers generate an output voltage, which is too high to directly feed the DC bus (typical 700–800 V), requiring a step-down DC–DC converter at their output.

13.5.2 Isolated DC–DC Converter Topologies

The second DC–DC stage of these high-power chargers is essentially the modular building blocks consisting of solutions given in Section 13.4.2.

13.6 PRACTICAL EXAMPLE

In this section, a practical design example for a level 2, 3.3 kW universal input two-stage PHEV battery charger, with an output voltage range of 200–450 V is given.

Figure 13.19 illustrates a 3.3 kW on-board battery charger designed by Delta-Q Technologies Corporation. The charger requirements and specifications are illustrated in Table 13.3.

A step-by-step design consideration and methodology will be reviewed in detail for both front-end PFC boost converter and isolated DC–DC converter.

13.6.1 Front-End PFC Boost Converter Design

13.6.1.1 Topology Selection

The first step for any converter design is topology selection. The topologies of choice for front-end PFC boost converters in level 2 chargers are discussed in Section 13.4.1.

The selected topology in this example is a two-channel interleaved boost converter, as illustrated in Figure 13.4.

The switching frequencies for the PFC and the DC-to-DC converter stages are selected to be 70 and 200 kHz, respectively. To achieve high efficiency (e.g., >97%) for the hard-switched interleaved PFC and limit the fundamental switching frequency ripple to below 150 kHz in order to meet the EMI requirements, a switching frequency of 70 kHz was selected.

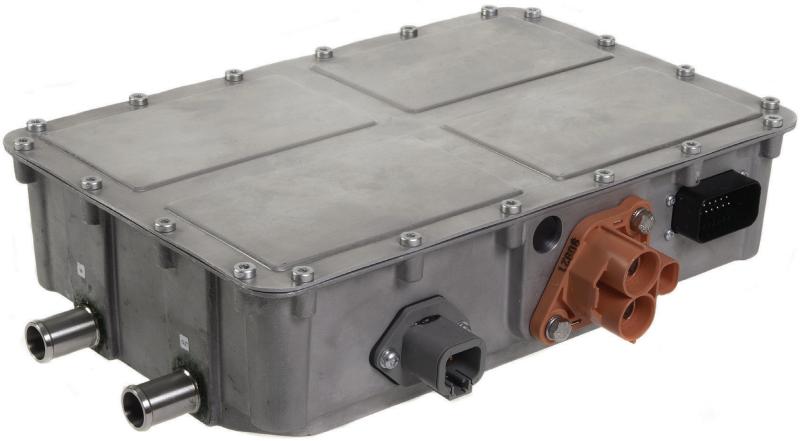

FIGURE 13.19 A 3.3 kW on-board PHEV battery charger designed by Delta-Q Technologies Corp.

In order to design the interleaved PFC converter, it can be treated as two conventional boost PFC converters with each operating at half of the load power rating. With this approach, all equations for the inductor, switch, and diode in the conventional PFC remain valid, since the stresses are unchanged with the only exception being the reduced ripple current through the output capacitors.

13.6.1.2 PFC Boost Converter Inductor Design

The minimum required boost inductor value in each phase for low line is given by Equation 13.7, where the minimum duty cycle at low line is defined by Equation 13.8 and ΔI_{L-LL} is the desired inductor current ripple at low line.

$$L_B = \frac{\sqrt{2}V_{in\_min}D_{min\_LL}}{f_s\Delta I_{L-LL}} \approx 400\mu H \tag{13.7}$$

TABLE 13.3
Level 2, 3.3 kW Charger Requirements and Specifications

Parameters	Value (Units)
Input AC voltage	85–265 (V)
Maximum input AC current	16 (A)
Power factor @ F.L. and 240 V input	99 (%)
AC input frequency	47–70 (Hz)
THD at full load and 240 V input	<5 (%)
Overall charger efficiency	Up to 94 (%)
Output DC voltage range	200–450 (V)
Maximum output DC current	11 (A)
Maximum output power	3.3 (kW)
Output voltage ripple	<2 (Vp-p)
Cooling	Liquid
Dimensions	273 × 200 × 100 (mm)
Mass/volume	6.2 (kg)/5.46 (L)
Operating temperature	–40°C to +105°C ambient
Coolant temperature	–40°C to +70°C

$$D_{\min\_LL} = 1 - \frac{\sqrt{2}V_{in\_min}}{V_{PFC\_bus}} \sin\left(\frac{\pi}{2}\right) \tag{13.8}$$

13.6.1.3 PFC Bus Capacitor Selection

The PFC bus capacitor is determined by Equation 13.9, where the maximum holdup time required for the PFC bus is given by Equation 13.10 and $\Delta V_{PFC\text{-}bus}$ is the intended low-frequency ripple across the PFC bus capacitor:

$$C_{PFC} = \frac{2P_o T_{Hold\_Up}}{V_{PFC\_bus}^2 - (V_{PFC\_bus} - \Delta V_{PFC\_bus})^2} \tag{13.9}$$

$$T_{Hold\_Up} = \frac{1}{4}\frac{1}{2f_{Line}} \tag{13.10}$$

In addition to the capacitor value, the capacitor ripple current handling must be considered as well. The high-frequency ripple current in the PFC capacitor is given by Equation 13.11, where I_o is given by Equation 13.12 and η_{PFC} is the efficiency of the PFC stage.

$$I_{C\_HF} = I_o \sqrt{\frac{16V_{PFC\_bus}}{6\pi\sqrt{2}V_{in\_min}} - \eta_{PFC}^2} \tag{13.11}$$

$$I_o = \frac{P_o}{V_{PFC\_bus}} \tag{13.12}$$

The low-frequency ripple current in the PFC capacitor is given by Equation 13.13.

$$I_{C\_LF} = \frac{I_o}{2} \tag{13.13}$$

13.6.2 Isolated DC–DC Converter Design

13.6.2.1 Topology Selection

The topologies of choice for front-end PFC boost converters in level 2 chargers are discussed in Section 13.4.2. The selected topology in this example is a full-bridge ZVS converter with trailing-edge PWM converter, as illustrated in Figure 13.12.

The full-bridge DC–DC converter was designed to operate at a PFC bus voltage, V_{PFC}, of 400 *V* and an output voltage, V_o, of 400 V at full load. Initially, a peak-to-peak output ripple current, ΔI_o, of 1 A was assumed. Including dead-time and duty cycle loss, an effective duty cycle of 0.75 was assumed.

13.6.2.2 Transformer Design

Following the assumptions made, the transformer turns ratio is determined to be 0.75 using Equation 13.14.

$$n_t = \frac{D_{eff}V_{in}}{V_o} \tag{13.14}$$

A custom planar-type ferrite transformer was designed using turns ratio of 12(Np):16(Ns).

13.6.2.3 Output Filter Inductor Design

An output filter inductor value of 400 µH was selected using Equation 13.14.

$$L_o = \frac{(V_{in}/n_t - V_o)D_{eff}}{\Delta I_d 2 f_s} \tag{13.15}$$

13.6.2.4 Resonant Inductor Design

The calculated resonant inductor is given in Equation 13.16. A 6-µH resonant inductor was selected, which is smaller as compared to the value calculated using Equation 13.16. A toroidal (iron powder core) inductor was used to obtain 4 µH and an additional 2 µH was obtained using the transformer leakage inductance.

$$L_R = \frac{n_t V_{in}(1 - D_{eff})}{4\Delta I_d f_s} = 8\ \mu H \tag{13.16}$$

13.7 WIRELESS CHARGERS

13.7.1 Introduction

On-board chargers are burdened by the need for a cable-and-plug charger, galvanic isolation of the on-board electronics, the size and weight of the charger, and safety and issues with operating in rain and snow. Wireless power transfer (WPT) is an approach that provides a means to address these problems and offers the consumers a seamless and convenient alternative to charging conductively. In addition, it provides an inherent electrical isolation and reduces on-board charging cost, weight, and volume [41].

A typical closed-loop inductive WPT charging system is illustrated in Figure 13.20 [42,43]. The basic principle of inductive WPT charging is that the two halves of the inductive coupling interface consist of the primary and secondary of a two-part transformer. The charger converts the low-frequency AC utility power to high-frequency AC power in the power conversion stage. The secondary side wirelessly receives high-frequency AC from the charger, which is converted to DC by a rectifier, which then supplies the battery pack.

A two-part transformer behaves like mutual-inductively coupled or magnetically coupled inductors configured such that a change in current flow through one winding induces a voltage across the ends of the other winding through electromagnetic induction, as shown in Figure 13.21.

The inductive coupling between two conductors is given by Equations 13.7 and 13.8.

$$v_1 = L_1 \frac{di_1}{dt} + M \frac{di_2}{dt} \tag{13.17}$$

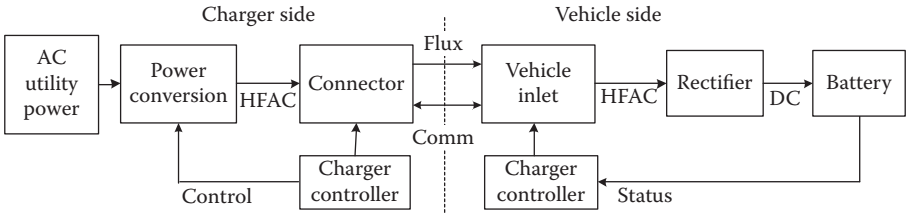

FIGURE 13.20 Typical closed-loop WPT charging systems.

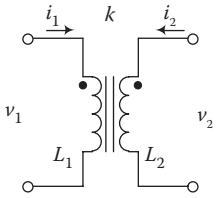

FIGURE 13.21 Coupled inductor circuit symbol.

$$v_2 = L_2 \frac{di_2}{dt} + M \frac{di_1}{dt} \tag{13.18}$$

In Equations 13.7 and 13.8, M denotes the mutual inductance, as given by Equation 13.9, where k is the coupling coefficient of the windings, or the quality of the magnetic circuit.

$$M = k\sqrt{L_1 L_2} \tag{13.19}$$

For a current I_1 in L_1, the open circuit voltage induced in L_2 is given by Equation 13.10.

$$V_{OC} = \omega M I_1 \tag{13.20}$$

With a short circuit on the right-hand side, the current is given by Equation 13.11.

$$I_{SC} = \frac{V_{OC}}{\omega L_1} = I_1 \frac{M}{L_2} \tag{13.21}$$

When the system is tuned at the operating frequency with a capacitor, the available power is V_{OC} I_{SC} multiplied by the circuit tuning resonant factor Q, and is given by Equation 13.12, where Q is given by Equation 13.13 [44].

$$P = \omega \frac{M^2}{L_2} I_1^2 Q = \omega L_1 I_1 I_1 \frac{M^2}{L_1 L_2} Q = V_1 I_1 k^2 Q \tag{13.22}$$

$$Q = \frac{\omega L}{R_L} \tag{13.23}$$

In Equation 13.12, the first two terms are the input voltage and current, the third term is the magnetic coupling factor, and the final term is the secondary circuit Q. The power that an inductive WPT system can produce is therefore dependent on the input voltage–ampere product (VA) to the primary pad, the quality of the magnetic circuit (k), and the quality of the secondary electric circuit (Q).

13.7.2 Inductive Charging

In the 1990s, electric vehicles used inductive charging. An inductive charger uses mutual inductance to transfer electrical energy from the source to the vehicle. This works much the way a transformer works. In this system, an insulated paddle containing an electrically energized primary coil is brought close to a secondary coil within the vehicle. The magnetic field of the primary coil then induces a charge in the secondary coil.

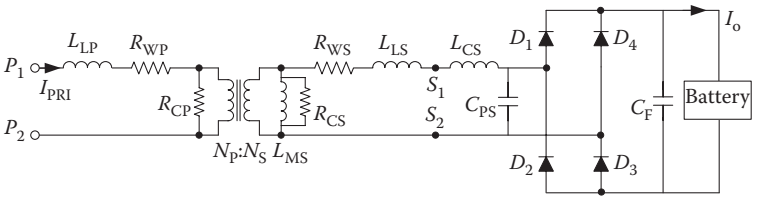

FIGURE 13.22 Inductive interface (paddle) equivalent circuit.

The charging paddle (the primary coil) of the Magne Charge inductively coupled charger was sealed in epoxy as was the secondary. The paddle inserted into the center of the secondary coil permitted charging of the EV1 without any contacts or connectors at either 6.6 or 50 kW. It should be noted that this system is connectorless, but not wireless.

The equivalent circuit parameters at the charge coupling interface for an IPT charger are shown in Figure 13.22.

13.7.3 Resonant Inductive Charging

Resonant inductive power transfer (RIPT) is the most popular current WPT technology [45,46]. It was pioneered by Nikola Tesla and has recently become popular again, enabled by modern electronic components. This technique uses two or more tuned resonant tanks resonating at the same frequency [47].

A typical schematic of an RIPT system is illustrated in Figure 13.23. The receiver and transmitter contain resonant capacitors, Cp and Cs. Various resonant compensation topologies are proposed in Reference 48. As noted in Reference 47, the primary functions of the resonant circuits include

- Maximizing the transferred power
- Optimizing the transmission efficiency
- Controlling the transmitted power by frequency variation
- Creating a certain source characteristic (current or voltage source)
- Compensating variation of the magnetic coupling
- Compensating the magnetizing current in the transmitter coil to reduce generator losses
- Matching the transmitter coil impedance to the generator
- Suppressing higher harmonics from the generator

Efficient resonant magnetic power coupling can be achieved at distances up to approximately 40 cm. RIPT systems have several advantages over IPT, including increased range, reduced EMI, higher-frequency operation, resonant switching of the inverter and receiver rectification circuitry, and higher efficiency. However, the main advantage of this concept is that the operating frequency is in the kHz range, which can be supported by current state-of-the-art power electronics technologies.

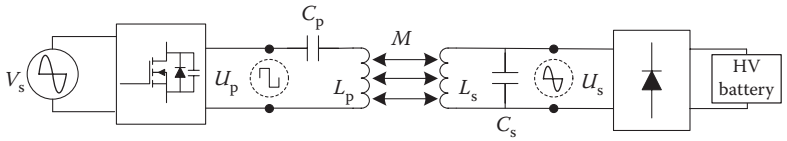

FIGURE 13.23 Simplified typical schematic of a resonant inductive charger.

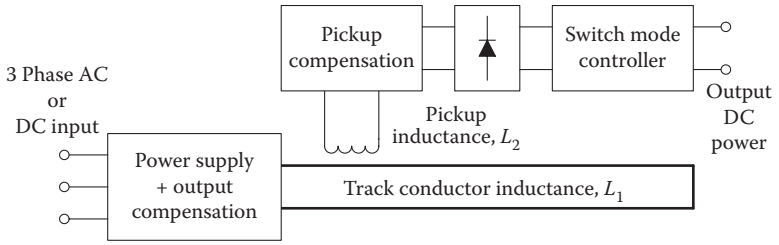

FIGURE 13.24 A typical on-line wireless power transfer system [49–58].

13.7.4 Roadway/On-Line Charging

The application of RIPT technology in public transit systems has been proposed in References 49–58. An on-line wireless power transfer system (OLPT) is illustrated in Figure 13.24. The concept is similar to RIPT; however, a lower resonant frequency is used and the technology has the potential for application at high power levels. Technologically, the primary coil is spread out over an area on the roadway and the power transfer happens at multiple locations within this area. Typically, the combination of the input side of the resonant converter along with the distributed primary windings is called the track and is on the road, and the secondary is called the pickup coil, which is in the vehicle. The system is supplied by a three-phase AC system, or high-voltage DC system. Considering both the short range of EVs and the associated cost of infrastructure, the feasibility of these charging systems might be unfavorable. However, one benefit is that due to frequent and convenient charging, vehicles can be built with a minimal battery capacity (about 20% compared to that of the conventional battery-powered electric vehicles), which can consequently minimize the weight and the price of the vehicle [56].

QUESTIONS AND PROBLEMS

13.1 What are the differences between AC charger and DC charger systems?

13.2 What are the classifications of chargers based on their power level?

13.3 What are the most common topologies for front-end AC–DC converters in a level 2 charger?

13.4 What are the most common topologies for front-end DC–DC converters in a level 2 charger?

13.5 Derive a formula to show the relationship between PF and THD.

13.6 In a conventional PFC boost converter operating in CCM, consider all components to be ideal. Let V_{in} be 85–265 V, $V_o = 400$ V (regulated), $P_o = 1650$ W, and $f_s = 70$ kHz. Calculate L_{min}, low-frequency and high-frequency ripple current in the output capacitors, and the capacitance value if the desired low-frequency voltage ripple at the output is assumed to be 10% of nominal output voltage.

13.7 Repeat problem 13.6 for a bridgeless boost converter and $P_o = 3300$ W.

13.8 In a ZVS full-bridge DC–DC converter topology with capacitive output filter, what are the modes of operation to be considered? Let $V_{in} = 400$ V, $V_o = 200$–450 V, $f_s = 200$ kHz, and $P_o = 3300$ W. Calculate L_{R_min}, low-frequency and high-frequency ripple current in the output capacitors, and the capacitance value if the desired low-frequency voltage ripple at the output is assumed to be 2% of nominal output voltage (300 V).

13.9 Use the parameters given in problem 13.8 for an LLC resonant DC–DC converter. Find the operating frequency range, resonant tank component values, and low-frequency and high-frequency ripple current in the output capacitors, and the capacitance value if the desired low-frequency voltage ripple at the output is assumed to be 2% of nominal output voltage (300 V).